

Magnetic impurities in a charge-ordered background

Sebastião dos Anjos Sousa-Júnior¹,* Raimundo R. dos Santos¹, and Natanael C. Costa¹
Instituto de Física, Universidade Federal do Rio de Janeiro Cx.P. 68.528, 21941-972 Rio de Janeiro RJ, Brazil

 (Received 9 September 2022; accepted 7 February 2023; published 21 February 2023)

We investigate how magnetic impurities may affect a system exhibiting a charge-density wave (CDW) in its ground state. We consider a disordered Hubbard-Holstein model with a homogeneous electron-phonon interaction but with a (randomly chosen) fraction of sites displaying a nonzero Coulomb repulsion U and perform state-of-the-art finite-temperature quantum Monte Carlo simulations. For a single magnetic impurity, charge-charge correlations hamper the spin-spin ones around the repulsive site, thus requiring a strong enough value of U to create nonnegligible antiferromagnetic (AFM) correlations. As the number of magnetic impurities increases, these AFM correlations become deleterious to CDW order and its features. First, the critical temperature is drastically reduced and seems to vanish $\sim 40\%$ of impurities (for fixed $U/\lambda = 2$), which we correlate with the classical percolation threshold. We also notice that just a small amount of disorder suffices to create a bad insulating state, with the suppression of both Peierls and spin gaps, even within the charge-ordered phase. Finally, we have also found that pairing correlations are enhanced at large doping, driven by the competition between CDW and AFM tendencies.

DOI: [10.1103/PhysRevB.107.075140](https://doi.org/10.1103/PhysRevB.107.075140)

I. INTRODUCTION

Over the past decades, much interest has been given to unveil the nature and interplay between long-range ordered phases in transition metal dichalcogenides (TMDs) [1–3]. Great experimental effort through different scenarios has been invested to understand the occurrence of a charge-density wave (CDW) and superconductivity (SC) in these compounds—from gate-induced [4] and hydrostatic pressure [5] to chemical doping [6] and substitutional disorder [7]—even though the emergence and competition between these phases are still open issues. Interestingly, the phase diagrams of TMDs [5] resemble those of doped high-temperature cuprate superconductors, which has raised the possibility of investigating pseudogap phenomena in the former to further understand the latter [8]. However, a remaining open question about TMDs, and more generally about the nature of the charge [9] and pairing interplay, is how spin-spin correlations may affect this competition, in other words, how repulsive electron-electron ($e-e$) and retarded electron-phonon ($e-ph$) interactions affect the ground state and thermodynamic properties of such compounds.

Within this context, TMDs provide odd opportunities to investigate this interplay. For instance, most of the $1T$ polytypes [5,10] exhibit flat bands, a feature that renders both $e-e$ and $e-ph$ interactions nonnegligible. Beyond this case, the effects of spin-spin correlations on CDW and SC phases may be investigated by systematically intercalating magnetic ions, such as Fe atoms, between layers of a given TMD. As a direct consequence of such a procedure, it has been established that a small amount of doping/intercalation is already enough to suppress the CDW order and change the SC critical temper-

ature [11,12]. In addition, the effects on transport properties have been examined, e.g., for NbSe₂ intercalated by Fe ions [13], providing evidence that electric current could be used to adjust the magnetic orientation of the spins, which can make this material suitable for spintronic devices. Other important features, such as the occurrence of the Kondo effect and its relevance to transport properties, are still under intense debate [14–16].

To investigate fundamental properties of such interacting compounds, one should examine the features of simplified effective Hamiltonians. In this framework, the single-band Hubbard-Holstein model (HHM) [17] considers the Coulomb repulsion between electrons as well as an indirect retarded electronic interaction due to an $e-ph$ coupling. The inclusion of these interactions may lead to electronic instabilities, with the enhancement of strong charge, spin, and/or pairing correlations, therefore capturing the interplay between CDW, antiferromagnetic (AFM), and/or SC phases. For instance, the ground state of the pure Holstein model on a half-filled square lattice has been extensively scrutinized [18–22], exhibiting a CDW for any $e-ph$ interaction [23]. However, this ordered phase is unstable under external parameters, with the enhancement of (conventional) pairing correlations when doping [24,25], pressure or strain [26,27], nonlinear $e-ph$ couplings [28–30], Anderson disorder [31], or phonon dispersion [32] take place. The addition of a repulsive Hubbard-like term to the Holstein model leads to similar behavior: The $e-e$ interaction suppresses double occupation, destroying the CDW phase, while enhancing AFM or pairing correlations [23,33].

In this paper, we examine a case interpolating between the pure Holstein model and the HHM, in the sense that an $e-e$ interaction is only considered on a fraction of sites/orbitals, i.e., when a percentage of sites are treated as $e-e$ interacting. Such a dilute-to-dense crossover may be a rough model for intercalated magnetic impurities on TMDs, with the $e-e$

*sebastiaojr@pos.if.ufrj.br

interacting sites playing the role of an intercalated magnetic site. Although most TMD polytypes exhibit geometries that may lead to frustration effects, here, we avoid these features, which would further increase the degree of complexity of our analysis [27,34]. Spin frustration would occur only at much higher concentrations of impurities (i.e., way beyond x_c), which is not the main goal of this paper. Therefore, to simplify our model, we investigate the stability of the well-known staggered CDW phase on the half-filled square lattice as the number of impurity sites increases. To this end, we perform unbiased quantum Monte Carlo (QMC) simulations aiming to analyze three main aspects: The behavior of charge and spin correlations (i) in the dilute regime—one or two magnetic impurities—and (ii) in the dense regime, as well as (iii) the behavior of thermodynamic quantities. Within such analyses, we expect to provide further insights about the nature of the charge ordered phase in the HHM. The paper is organized as follows: The model and methodology are outlined in the next section, while our results are presented in Secs. III and IV. Our final remarks are given in Sec. V.

II. MODEL AND METHODS

The HHM describes electrons on a lattice interacting with each other through both a direct on-site Coulomb repulsion and a coupling with phononic degrees of freedom. In the standard second quantization formalism, the Hamiltonian reads

$$\begin{aligned} \mathcal{H} = & -t \sum_{\langle \mathbf{ij} \rangle, \sigma} (c_{i\sigma}^\dagger c_{j\sigma} + \text{H.c.}) - \mu \sum_{i, \sigma} n_{i\sigma} + \sum_i U_i n_{i\uparrow} n_{i\downarrow} \\ & + \sum_i \left(\frac{\hat{P}_i^2}{2M} + \frac{M\omega_0^2 \hat{X}_i^2}{2} \right) - g \sum_{i, \sigma} n_{i\sigma} \hat{X}_i, \end{aligned} \quad (1)$$

where $c_{i\sigma}^\dagger$ ($c_{i\sigma}$) are creation (annihilation) operators of electrons with spin σ at a given site \mathbf{i} , while $n_{i\sigma} \equiv c_{i\sigma}^\dagger c_{i\sigma}$ are number operators. Here, the sums run over a two-dimensional square lattice under periodic boundary conditions, with $\langle \mathbf{ij} \rangle$ denoting nearest-neighbor sites. The first two terms on the right-hand side of Eq. (1) correspond to the kinetic energy of electrons and their chemical potential μ term, respectively, while the on-site Coulomb repulsion between electrons is included through the third term. Notice that we have introduced a site dependence on the interaction strength U_i , which is described in detail below. The phonon degrees of freedom appear in the fourth term as quantum harmonic oscillators with frequency ω_0 (as an Einstein model), with \hat{P}_i and \hat{X}_i being conjugate momentum and position operators, respectively. The last term corresponds to the electron-ion coupling, whose strength is g . Hereafter, we define the mass of the ions M and the lattice and Boltzmann constants as unity, while using the hopping integral t to define the scale of energy.

At this point, it is important to recall that the electron-phonon coupling leads to *polarons*, i.e., quasiparticles formed by electrons dressed by a cloud of phonons, whose characteristic energy scale is $\lambda = g^2/\omega_0^2$. Therefore, it is convenient to adopt λ/t as the strength of the e - ph interaction. In addition, we also define ω_0/t as the adiabaticity ratio. Throughout this paper, we have fixed $\lambda/t = 2$ and $\omega_0/t = 1$, while varying

the Coulomb strength U/t and the fraction x of magnetic impurities.

We investigate the properties of Eq. (1) by performing finite-temperature determinant QMC (DQMC) simulations [18,35–37]. The DQMC approach is an unbiased method based on the decoupling of the noncommuting terms of the Hamiltonian in the partition function by Trotter-Suzuki decomposition, i.e., by discretizing the inverse temperature into small imaginary-time steps $\beta = M\Delta\tau$. For the Hubbard-Holstein Hamiltonian, such a procedure leads to

$$\begin{aligned} \mathcal{Z} &= \text{Tr} \exp(-\beta \hat{\mathcal{H}}) \\ &\approx \text{Tr} [\dots \exp(-\Delta\tau \hat{\mathcal{H}}_K) \exp(-\Delta\tau \hat{\mathcal{H}}_{\text{ph}}) \\ &\quad \times \exp(-\Delta\tau \hat{\mathcal{H}}_{e-ph}) \exp(-\Delta\tau \hat{\mathcal{H}}_U) \dots], \end{aligned} \quad (2)$$

where \mathcal{H}_K , \mathcal{H}_{ph} , \mathcal{H}_{e-ph} , and \mathcal{H}_U correspond to the kinetic, bare phonon modes, e - ph coupling, and Hubbard interaction terms, respectively. The above breakup introduces errors of $O(\Delta\tau^2)$, but becomes exact when $\Delta\tau \rightarrow 0$. For the range of coupling constants considered here, we have typically set $\Delta\tau t = 0.1$ to determine the number of time slices M for each temperature. Further, we have checked that the Trotter error $O(\Delta\tau^2)$ does not affect our results significantly.

To proceed, we employ a Hubbard-Stratonovich transformation to obtain the $\exp(-\Delta\tau \hat{\mathcal{H}}_U)$ operators as quadratic forms but with the price of adding new degrees of freedom $s_{i,l}$: The Hubbard-Stratonovich fields. The bosonic and fermionic traces Tr lead to

$$\begin{aligned} \mathcal{Z} &\propto \int \mathcal{D}\{x_{i,l}\} \mathcal{D}\{s_{i,l}\} \exp(-\Delta\tau S_B) \\ &\quad \times \Pi_\sigma [\det(I + B_M^\sigma B_{M-1}^\sigma \dots B_1^\sigma)], \end{aligned} \quad (3)$$

with $x_{i,l}$ being phonon degrees of freedom, and S_B the bare phonon action:

$$S_B = \frac{\omega_0^2}{2} \sum_i \sum_{l=1}^M \left[\frac{1}{\omega_0^2 \Delta\tau^2} (x_{i,l} - x_{i,l+1})^2 + x_{i,l}^2 \right], \quad (4)$$

and the matrices $B_l^\sigma \equiv B_l^\sigma(x_{i,l}, s_{i,l})$ are defined as

$$\begin{aligned} B_l^\sigma &= \exp(-\Delta\tau \hat{\mathcal{H}}_K) \exp(-\Delta\tau \hat{\mathcal{H}}_{\text{ph}}) \exp(-\Delta\tau \hat{\mathcal{H}}_{e-ph}) \\ &\quad \times \exp(-\Delta\tau \hat{\mathcal{H}}_U). \end{aligned} \quad (5)$$

The integrals $\int \mathcal{D}\{x_{i,l}\} \mathcal{D}\{s_{i,l}\}$, i.e., the bosonic traces, are performed by Monte Carlo methods. Within this approach, one may obtain both equal-time and unequal-time Green's functions $\mathcal{G}^\sigma(\tau, \tau')$ and, therefore, any higher-order correlation functions. Further methodological details may be found, e.g., in Refs. [38–40].

Given this, we investigate the magnetic properties of the Hamiltonian in Eq. (1) through the spin-spin correlation functions:

$$C_{\text{spin}}(\mathbf{i}, \mathbf{j}) = \langle (n_{i\uparrow} - n_{i\downarrow})(n_{j\uparrow} - n_{j\downarrow}) \rangle, \quad (6)$$

while its charge response is examined through the charge-charge ones:

$$C_{\text{charge}}(\mathbf{i}, \mathbf{j}) = \langle (n_{i\uparrow} + n_{i\downarrow})(n_{j\uparrow} + n_{j\downarrow}) \rangle. \quad (7)$$

We probe the occurrence of charge instabilities through the behavior of the charge structure factor:

$$S_{\text{cdw}}(\mathbf{q}) = \frac{1}{N} \sum_{\mathbf{i}, \mathbf{j}} \exp[-i\mathbf{q} \cdot (\mathbf{i} - \mathbf{j})] C_{\text{charge}}(\mathbf{i}, \mathbf{j}), \quad (8)$$

and its correlation ratio:

$$R_{\text{cdw}}(L) = 1 - \frac{S_{\text{cdw}}(\mathbf{Q} + \delta\mathbf{q})}{S_{\text{cdw}}(\mathbf{Q})}, \quad (9)$$

with $N = L \times L$ being the number of sites, $|\delta\mathbf{q}| = 2\pi/L$, and $\mathbf{Q} = (\pi, \pi)$. The crossing of $R_{\text{cdw}}(L)$ for different lattice sizes, together with their finite-sized scaling analyses, provides estimates for the location of the critical region [41–45].

Finally, we also examine the pairing response by means of the finite-temperature pair susceptibility:

$$\chi_{\text{sc}}(\alpha) = \frac{1}{N} \sum_{\mathbf{i}, \mathbf{j}} \int_0^\beta \langle \Delta_\alpha(\mathbf{i}, \tau) \Delta_\alpha^\dagger(\mathbf{j}, 0) \rangle d\tau, \quad (10)$$

with

$$\Delta_\alpha(\mathbf{i}, \tau) = \frac{1}{2} \sum_{\mathbf{a}} f_\alpha(\mathbf{a}) c_{\mathbf{i}\downarrow}(\tau) c_{\mathbf{i}+\mathbf{a}\uparrow}(\tau), \quad (11)$$

where $c_{i\sigma}(\tau) = \exp(\tau\mathcal{H}) c_{i\sigma} \exp(-\tau\mathcal{H})$, and $f_\alpha(\mathbf{a})$ is the pairing form factor for a given wave symmetry $\alpha = s$ or d . One expects the dominant pairing susceptibility to diverge most strongly as the temperature is lowered. However, as we will see below, we were unable to reach temperatures low enough to resolve the divergences for different pairing symmetries. An alternative probe [23,46] is to remove the noninteracting (vertex) contribution to the susceptibility $\bar{\chi}_{\text{sc}}(\alpha)$ and define the *effective* response as

$$\chi_{\text{sc}}^{\text{eff}} = \chi_{\text{sc}}(\alpha) - \bar{\chi}_{\text{sc}}(\alpha). \quad (12)$$

With this, a positive (negative) value of $\chi_{\text{sc}}^{\text{eff}}$ corresponds to an enhancement (weakening) of an attractive pair channel for the α symmetry.

To describe the effects of magnetic impurities in a CDW environment, here, we deal with the half-filled square lattice, which is known to exhibit a charge-ordered ground state for any finite e - ph coupling, $\lambda/t > 0$. We model the impurities by allowing for random distributions of $U_i > 0$ on the lattice, for a given fraction x of the sites, as

$$U_i = \begin{cases} U & \text{with probability } x; \\ 0 & \text{with probability } (1 - x). \end{cases} \quad (13)$$

To ease the discussion, in what follows, we present the results for the dilute regime (i.e., one and two impurities) separate from those for the dense regime of many impurities. All results for the dense limit were obtained by averaging the quantities over 100–200 disorder configurations.

III. RESULTS FOR THE DILUTE CASE

A. Single impurity

We start with the investigation of the single-impurity case. For the sake of comparison, we recall that, when a magnetic impurity is placed in a *metallic* environment ($\lambda = 0$), AFM correlations are enhanced around it, whose strength

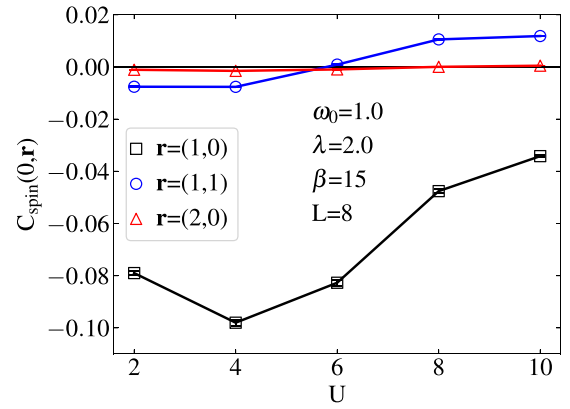


FIG. 1. Spin-spin correlation functions between the impurity site and the three nearest neighbors, as a function of U .

decays with distance; in addition, as the number of impurities increases, this AFM cloud evolves toward a long-range ordered configuration [47,48]. In a CDW background, on the other hand, such staggered spin-spin correlations are drastically suppressed or even destroyed, as displayed in Fig. 1. Notice that, for small values of U , first-, second-, and third-neighbor spin-spin correlations exhibit negative responses, in stark contrast with the previous picture of an AFM cloud in the metallic case. To understand this difference, note that the effects brought about by a single U impurity in a charge-ordered background start with the broken twofold degeneracy of the CDW ground state on a square lattice: If the impurity is located on, say, the α sublattice, the CDW is stabilized on the β sublattice. The very weak spin correlations between the impurity site and its second and third neighbors is accounted for by the fact these sites belong to the α sublattice, hence with a very small local moment when U is small. More robust spin correlations with sites on the β sublattice, on the other hand, indicate a redistribution of the spin cloud surrounding the impurity. As U increases, nearest-neighbor correlations are first strengthened and then weakened [49], which is accompanied by a reversal of the sign of $c(1, 1)$ (blue circles in Fig. 1): This indicates a new redistribution such that AFM correlations become dominant locally, with the creation of an AFM cloud around the impurity. That is, in the presence of a CDW background, a large U is needed to generate an AFM cloud around the impurity; such a critical value of U has a strong dependence on the e - ph coupling strength (not shown). The occurrence of this AFM cloud is what leads to the emergence of long-range order for the many-impurity case, discussed below.

B. Two impurities

Let us now consider the case of two impurities and examine how the relative position between the $U_i \neq 0$ centers affects the overall properties. Figure 2 shows the spin-spin correlation functions between two impurity sites on the same sublattice as a function of their distance. Like the single-impurity case, the profile of correlations is very sensitive to the magnitude of U . For $U = 2$ and when the impurity sites are nearest neighbors within the same sublattice (NN α), the impurity spins are weakly antiferromagnetically correlated, while for

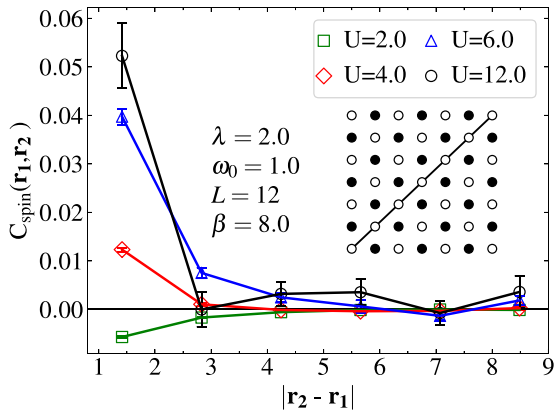


FIG. 2. Spin-spin correlation functions between two impurities on the same sublattice, as a function of the distance $|\mathbf{r}_2 - \mathbf{r}_1|$ between them and for different values of U/t .

$U = 4$, they are already ferromagnetically correlated. As U is increased further, the profile changes considerably, in the sense that the period of oscillation seems to decrease.

The first row of Fig. 3 shows the profile of double occupancy:

$$D_i \equiv \langle n_{i\uparrow} n_{i\downarrow} \rangle, \quad (14)$$

with $D_i \in [0, \frac{1}{2}]$ at half-filling, for different values of U ; the impurity sites are placed on the same sublattice, at $(x, y) = (0, 0)$ and $(x, y) = (2, 2)$. As expected, the sublattice symmetry is broken, with D_i always being larger on the sublattice not containing the impurities. Further, as U increases, D_i on the impurity sites decreases steadily. The middle row of Fig. 3 shows the local moment:

$$\langle m_i^2 \rangle \equiv \langle (n_{i\uparrow} - n_{i\downarrow})^2 \rangle = [\langle n_i \rangle - 2D_i], \quad (15)$$

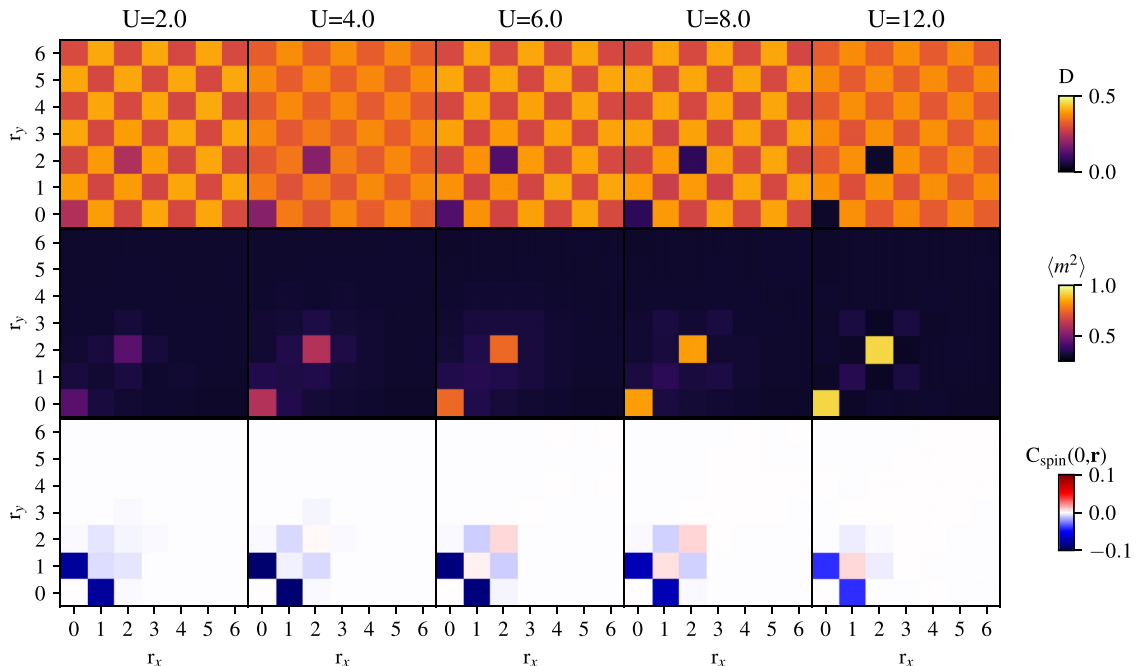


FIG. 3. Real-space results for the double occupancies (upper panels), local moments (middle panels), and spin-spin correlation functions (lower panels) for a system with two impurities, one in the origin and the other the coordinates $(2, 2)$. Here, we fixed $L = 12$ and $\beta t = 8.0$.

with $\frac{1}{N} \sum_i \langle n_i \rangle = n = 1$ at half-filling, for different values of U . It is clear that the local moment is suppressed on all sites, except on the impurity ones. We may thus conclude that there is an increasing tendency to occupy the impurity sites with a single spin.

The bottom row of Fig. 3 shows the spin correlations between an impurity site (placed at the origin) and sites with coordinates $\mathbf{r} \equiv (x, y)$, in the presence of the second impurity at $(x, y) = (2, 2)$. If U is small, the sites surrounding the impurity tend to align antiferromagnetically with it, which includes, although less intense, the other impurity; in view of the analysis of the single-impurity case, the presence of a second impurity strengthens the AFM correlations around the impurities. However, for increasing values of U , the correlations along the diagonal display oscillations with U . Further, the period of oscillation depends on the relative position between the sites, reminiscent of an RKKY-like interaction, but having in mind that this occurs in the presence of a CDW background.

IV. THE DENSE REGIME

A. CDW transition

In the previous section, we established that AFM correlations can overcome the charge order locally by increasing U in a single impurity or in two repulsive sites. In this section, we aim to determine the minimum concentration of U sites required to destroy the CDW for $U > \lambda$. Since the presence of impurity sites tends to deplete doubly occupied sites, a decrease in the CDW critical temperature is expected to occur for increasing $x = N_{\text{imp}}/N$, where N_{imp} is the number of impurity sites with $U \neq 0$.

For the many-impurity case, we recall that the quantities of interest are obtained after performing configurational

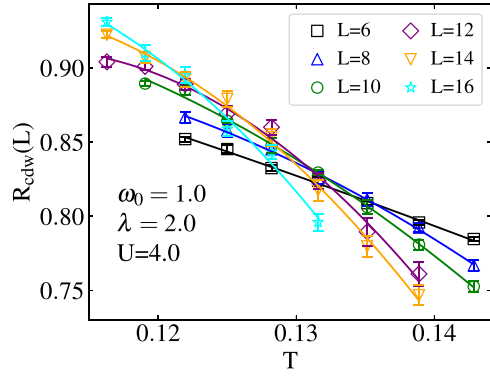


FIG. 4. The charge-density wave (CDW) correlation ratio [Eq. (9)] for fixed ω_0 , λ , and U as a function of temperature, for $x = 0.2$ and different lattice sizes L . The crossings provide estimates for T_c .

averages. Figure 4 shows the configurationally averaged CDW correlation ratio $R_{\text{cdw}}(L)$ [Eq. (9)] as a function of temperature, for different system sizes. The temperatures at which two curves, $R_{\text{cdw}}(L)$ and $R_{\text{cdw}}(L - \Delta L)$, intersect provides an estimate $T_c(L, L - \Delta L)$. Figure 5 exhibits these crossings for $U = 4$ and 6, and for fixed $\Delta L = 4$, from which we may extrapolate toward the critical temperature in the thermodynamic limit (see, e.g., the filled symbols). By extrapolating these estimates for $1/L \rightarrow 0$, we obtain the phase diagrams T_c vs x displayed in Fig. 6, from which we see that T_c decreases with increasing x , as expected. Further, a polynomial fitting to the data for $U = 4$ provides an estimate for the critical disorder concentration above which there is no CDW at finite temperatures as $x_c = 0.41 \pm 0.04$. By contrast, for $U = 6$, the data for $T_c(x)$ suffer from the severe minus-sign problem in the regime of low temperatures and large U , and we were unable to provide an estimate for x_c in this case.

Nonetheless, it is interesting to note that the $U \neq 0$ sites play the role of disordering agents as far as CDW order is concerned, so that x corresponds to the concentration $1 - p$ of inactive sites in ordinary percolation [50]; given that the critical site percolation threshold for the square lattice is $p_c = 0.59$ (see, e.g., Ref. [50]), our estimate $x_c = 0.41$ may indicate a major role played by geometrical constraints. This should

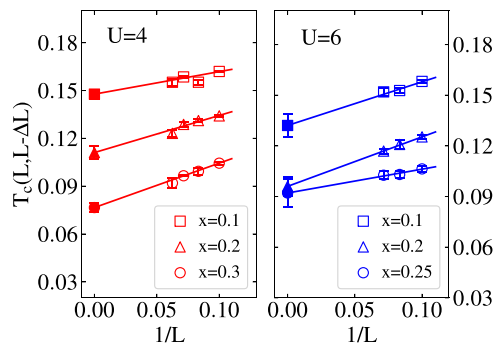


FIG. 5. Finite-sized scaling plots of the estimated charge-density wave (CDW) critical temperatures as determined from intersects such as those in Fig. 4, using $\Delta L = 4$; see text. Empty symbols are the estimates, and filled symbols are the extrapolated values.

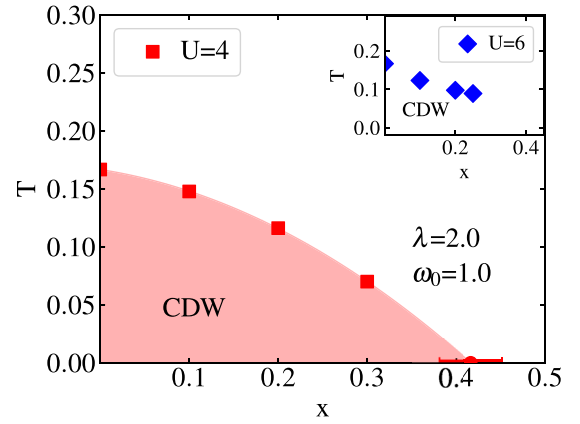


FIG. 6. The charge-density wave (CDW) critical temperature as a function of impurity concentration, for $U/t = 4$, and the same parameters of Fig. 5. The border of the shaded region is drawn from a polynomial fit to the data, from which the error bar around $x = 0.41$ is inferred. Inset: Data from simulations with $U = 6$; see text. In both plots, the error bars are smaller than the data points.

be contrasted with a recent study of the Hubbard model on a disordered Lieb lattice, which shows that the concentration threshold for magnetism is strongly dependent on the on-site repulsion [48]. For the present case, it is not a coincidence that our x_c is close to the geometric percolation threshold of the square lattice. One may understand this from the results of the single- and two-impurity cases. As discussed in Fig. 1, an AFM cloud is not formed when $U/t = 4$ and $\lambda/t = 2$, requiring that impurities should be sited side-by-side to have strong spin-spin correlations. Indeed, this picture is confirmed in the two-impurity case, where Figs. 2 and 3 show a drastic suppression of the spin-spin correlation functions for $U/t \lesssim 8$. That is, due to these short-range correlations, one may expect the CDW phase to be destroyed close to the classical geometric percolation threshold, even at moderately large values of U/λ . Therefore, x_c should be unchanged for $U/t = 6$, although the minus-sign problem prevents us from presenting numerical data.

B. The insulating state

In a clean system ($x = 0$), the temperature-driven CDW transition leads to an insulating state at half-filling, characterized by a Peierls gap and absence of SC [18,22,32]. We will now discuss how the presence of repulsive centers affects the transition to the insulating state. To this end, we resort to several quantities such as the double occupancy D [Eq. (14)], the kinetic energy E_k , the compressibility κ , and the uniform static spin susceptibility χ_{sp} . The two latter quantities are evaluated using the fluctuation-dissipation theorem [51,52]:

$$n^2 \kappa = \frac{dn}{d\mu} = \beta (\langle n^2 \rangle - \langle n \rangle^2), \quad (16)$$

and

$$\chi_{\text{sp}} = \frac{\partial m}{\partial h} = \frac{\beta}{N} \sum_{\mathbf{i}, \mathbf{j}} C_{\text{spin}}(\mathbf{i}, \mathbf{j}). \quad (17)$$

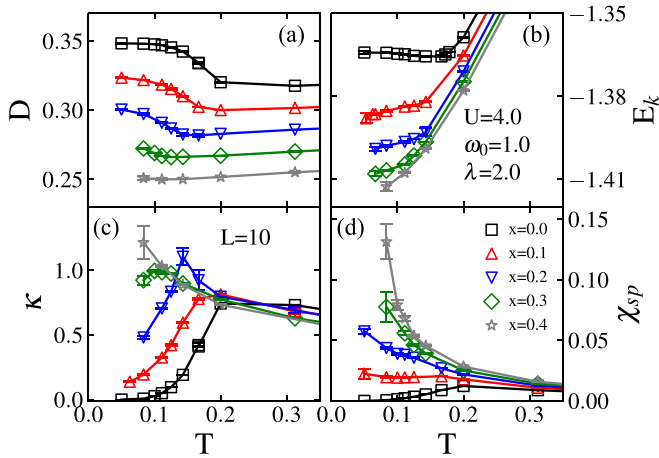


FIG. 7. (a) Double occupancy, (b) kinetic energy, (c) compressibility, and (d) uniform static spin susceptibility as functions of temperature T/t . Each curve is for a given impurity concentration, and all data are for fixed values of ω_0 , λ , and U .

Further analyses of these quantities may provide signatures of the crossover into a bad-metallic phase, as discussed in Ref. [53].

Figure 7(a) displays the behavior of the double occupancy as a function of temperature. For a CDW ground state, one expects a large value of D below $T \lesssim T_c$, while for a noninteracting metallic state, one has $D = 0.25$. Given this, notice that a peak in $\partial D(x, T)/\partial T$ appears for temperatures close to critical ones (see, e.g., Fig. 6), with the exception of $x = 0.4$, which presents $D \approx 0.25$ at low T . This is in agreement with our previous analysis, for the destruction of the CDW ground state for $x_c \approx 0.4$. Similar observations apply to the compressibility [Fig. 7(c)], for which the change in slope is accompanied by a peak whose positions decrease with increasing disorder.

However, the behavior of the kinetic energy, exhibited in Fig. 7(b), is more subtle. The black square symbols show its behavior for the clean case, where the ground state has a well-formed Peierls gap. For such a case, notice that the kinetic energy exhibits a slight increase for $T \lesssim T_c$, clearly showing an insulating behavior. In the presence of disorder, however, the kinetic energy still decreases within the insulating phase, although at a smaller rate than in the metallic phase. That is, we still have an insulating phase but a bad insulator, when compared with the Peierls one. We shall return to this discussion below.

Finally, Fig. 7(d) shows the temperature dependence of the uniform spin susceptibility for different impurity concentrations. For the clean system, the susceptibility goes to zero exponentially, reflecting the presence of a spin gap due to the doubly occupied sites forming the CDW state. As discussed before, the impurities tend to form AFM clouds around them by depleting the doubly occupied sites. For several impurities, however, these clouds display no long-range AFM order, so that a uniform magnetic field may easily polarize the local moments at the impurity sites, and a Curie-like magnetic response sets in as x increases, explaining the disappearance of the spin gap.

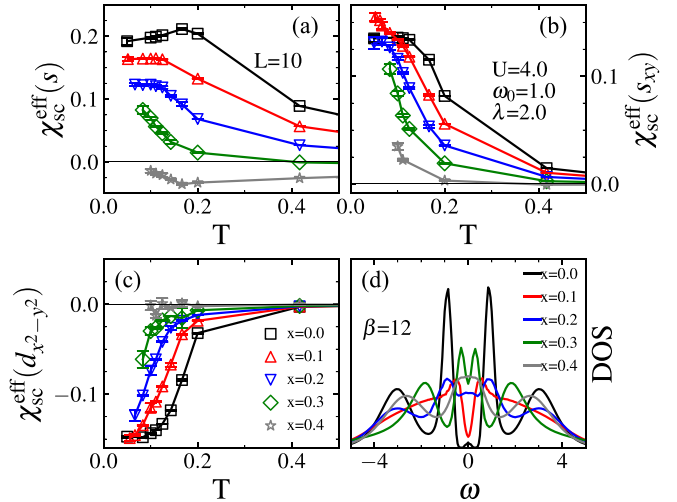


FIG. 8. Effective pairing susceptibility χ_{sc}^{eff} as a function of T for (a) s -wave, (b) s_{xy} -wave, and (c) $d_{x^2-y^2}$ -wave channels. Panel (d) shows the density of states (DOS) for $\beta/t = 12$ and several impurity concentrations. In each panel, the curves are for the given impurity concentrations, and all data are for fixed values of ω_0 , λ , and U .

C. Superconducting and spectral properties

Having established that magnetic impurities destroy the CDW insulating state, one may wonder whether this can favor superconducting correlations. To check this, we have calculated the effective pairing susceptibility $\chi_{sc}^{\text{eff}}(\alpha)$ for s -, s_{xy} -, and $d_{x^2-y^2}$ -wave symmetries; when this quantity is positive, an attractive channel sets in. Figures 8(a)–8(c) show the temperature dependence of the effective pairing susceptibility, from which we may rule out any pairing tendencies in the $d_{x^2-y^2}$ symmetry [panel (c)]—notice that χ_{sc}^{eff} is strongly suppressed as the temperature is lowered for all x . For the s - and s_{xy} -wave channels, on the other hand, the dirty system displays a behavior different from the clean one: χ_{sc}^{eff} increases as T decreases.

Although the pairing tendency is enhanced with the presence of impurities in a CDW background, pairing correlations cannot drive the system to a long-range superconducting ordered state in the regime of e - ph coupling considered here; a much larger λ is required to unequivocally reach long-range order. This is evidenced by the stabilization of χ_{sc}^{eff} at low temperatures, around the critical CDW temperature—long-range order would require a divergence in χ_{sc}^{eff} , which does not seem to occur for the range of temperatures analyzed. By contrast, in the absence of a CDW background, for $x > x_c$, $\chi_{sc}^{\text{eff}} > 0$ may be interpreted as favoring the formation of a superconducting phase. Unfortunately, for $x \gtrsim x_c$, the average fermionic sign is small, thus preventing analyses at low temperatures. At any rate, it is interesting to notice that, for $x = 0.4$, the only attractive pairing channel is the s_{xy} wave. That is, a superconducting state emerging in this region would display a pairing symmetry different from the standard on-site s wave, due to the Coulomb e - e interaction, in agreement with Refs. [23,33].

Finally, it is also worth examining the spectral properties of the system. We compute the density of states (DOS) by

performing an analytic continuation of the imaginary time-dependent Green's function, using the maximum entropy method [54]; this amounts to inverting the integral equation:

$$\mathcal{G}(\mathbf{r}_{ij} = 0, \tau) = \int d\omega N(\omega) \frac{\exp(-\omega\tau)}{\exp(\beta\omega) + 1}, \quad (18)$$

with \mathbf{r}_{ij} denoting the relative displacement between sites, and $N(\omega)$ is the sought DOS. Figure 8(d) shows the evolution of the DOS as the impurity concentration increases, for fixed $\beta/t = 12$. We see that disorder suppresses the Peierls gap present in the clean system, even for a small amount of impurities, e.g., for $x = 0.10$. Although it seems contradictory with the compressibility results in Fig. 7(c), which shows an insulating state for these values of x and T , it gives support for the results of Fig. 7(d), which suggests the appearance of localized states. Therefore, the scenario brought about by these results is that magnetic impurities suppress the Peierls gap by creating in-gap localized states, which in turn enhance magnetic correlations while destroying the CDW background at the percolation threshold.

V. CONCLUSIONS

We have studied the effect of magnetic impurities interacting with a CDW background, stabilized by e - ph coupling within the Holstein model scenario. The impurities are modeled by assigning a repulsive Hubbard U coupling to a site, which tends to favor the formation of a local moment, and we have considered a square lattice with a half-filled electronic band.

By first analyzing the dilute regime (one and two impurities), we have established that, unlike the metallic case, only for large U , the local moment is significant, and an AFM cloud forms around the isolated impurity site; this results from depleting nearby doubly occupied sites. When two impurities are placed on the same sublattice, spin correlations between them oscillate with U , reminiscent of an RKKY behavior. However, these correlations are strongly suppressed with distance, so that only nearest or next-nearest neighbors are relevant. In the dense regime, the impurities lower the critical temperature for CDW formation, which vanishes at some critical impu-

rity concentration x_c . Interestingly, our data for $U = 4$ yield $x_c \approx 0.4$, consistent with the classical percolation threshold for the square lattice (0.41). That is, due to the short-range charge-charge correlations the destruction of the CDW phase depends on geometrical aspects.

However, the CDW state that emerges when magnetic impurities are present is not a regular Peierls one. We have also established that the Peierls and the spin gaps are both suppressed by even a small amount of impurities. The occurrence of such a bad insulating phase is due to localized states at the Fermi level filling the gap, whose local moments, in turn, give rise to a Curie-like magnetic response. For $x \lesssim x_c$, these magnetic impurities cannot suppress the CDW background but may drastically change thermodynamic properties, such as the average kinetic energy.

Our data also show that superconducting correlations are enhanced in the s and s_{xy} channels, as a result of suppression of the CDW state. This is consistent with experimental findings [11] of an increase in the superconducting temperature with intercalation of Fe in CDW materials. For $x \gtrsim x_c$, when magnetic impurities destroy the CDW background, we expect that long-range order should emerge, but for nonlocal (not on-site) pairs, as an effect of the e - e interaction. In closing, we note that it has been recently suggested [31] that Anderson-like disorder in the Holstein model also gives rise to an enhancement of superconducting correlations at low temperatures, in agreement with our overall findings that disorder significantly disturbs the CDW state and leads to pairing.

ACKNOWLEDGMENTS

Financial support from the Brazilian Agencies CAPES, CNPq, and FAPERJ, and Instituto Nacional de Ciéncia e Tecnologia de Informação Quântica (INCT-IQ) is gratefully acknowledged. N.C.C. and S.A. Sousa-Júnior acknowledge PRACE for awarding them access to Marconi at CINECA, Italy. N.C.C. acknowledges financial support from CNPq, Grant No. 313065/2021-7, and from FAPERJ—Fundação Carlos Chagas Filho de Amparo Pesquisa do Estado do Rio de Janeiro, Grant No. 200.258/2023 (SEI-260003/000623/2023).

-
- [1] S. Manzeli, D. Ovchinnikov, D. Pasquier, O. V. Yazyev, and A. Kis, 2D transition metal dichalcogenides, *Nat. Rev. Mater.* **2**, 17033 (2017).
- [2] X. Zhu, Y. Cao, J. Zhang, E. W. Plummer, and J. Guo, Classification of charge density waves based on their nature, *Proc. Natl. Acad. Sci. USA* **112**, 2367 (2015).
- [3] X. Zhu, J. Guo, J. Zhang, and E. W. Plummer, Misconceptions associated with the origin of charge density waves, *Adv. Phys.: X* **2**, 622 (2017).
- [4] L. J. Li, E. C. T. O'Farrell, K. P. Loh, G. Eda, B. Özyilmaz, and A. H. Castro Neto, Controlling many-body states by the electric-field effect in a two-dimensional material, *Nature (London)* **529**, 185 (2016).
- [5] A. F. Kusmartseva, B. Sipos, H. Berger, L. Forró, and E. Tutiš, Pressure Induced Superconductivity in Pristine 1T-TiSe₂, *Phys. Rev. Lett.* **103**, 236401 (2009).
- [6] K. E. Wagner, E. Morosan, Y. S. Hor, J. Tao, Y. Zhu, T. Sanders, T. M. McQueen, H. W. Zandbergen, A. J. Williams, D. V. West, and R. J. Cava, Tuning the charge density wave and superconductivity in Cu_xTaS₂, *Phys. Rev. B* **78**, 104520 (2008).
- [7] L. Li, X. Deng, Z. Wang, Y. Liu, M. Abeykoon, E. Dooryhee, A. Tomic, Y. Huang, J. B. Warren, E. S. Bozin *et al.*, Superconducting order from disorder in 2H-TaSe_{2-x}S_x, *npj Quantum Mater.* **2**, 11 (2017).
- [8] U. Chatterjee, J. Zhao, M. Iavarone, R. Di Capua, J. P. Castellán, G. Karapetrov, C. D. Malliakas, M. G. Kanatzidis, H. Claus, J. P. C. Ruff *et al.*, Emergence of coherence in the charge-density wave state of 2H-NbSe₂, *Nat. Commun.* **6**, 6313 (2015).
- [9] M. M. Ugeda, A. J. Bradley, Y. Zhang, S. Onishi, Y. Chen, W. Ruan, C. Ojeda-Aristizabal, H. Ryu, M. T. Edmonds, H.-Z. Tsai *et al.*, Characterization of collective ground states in single-layer NbSe₂, *Nat. Phys.* **12**, 92 (2016).

- [10] Y. I. Joe, X. M. Chen, P. Ghaemi, K. D. Finkelstein, G. A. de la Peña, Y. Gan, J. C. T. Lee, S. Yuan, J. Geck, G. J. MacDougall *et al.*, Emergence of charge density wave domain walls above the superconducting dome in $1T$ -TiSe₂, *Nat. Phys.* **10**, 421 (2014).
- [11] Z. Dai, Q. Xue, Y. Gong, C. G. Slough, and R. V. Coleman, Scanning-probe-microscopy studies of superlattice structures and density-wave structures in $2H$ -NbSe₂, $2H$ -TaSe₂, and $2H$ -TaS₂ induced by Fe doping, *Phys. Rev. B* **48**, 14543 (1993).
- [12] D. Yan, Y. Lin, G. Wang, Z. Zhu, S. Wang, L. Shi, Y. He, M.-R. Li, H. Zheng, J. Ma *et al.*, The unusual suppression of superconducting transition temperature in double-doping $2H$ -NbSe₂, *Supercond. Sci. Technol.* **32**, 085008 (2019).
- [13] N. L. Nair, E. Maniv, C. John, S. Doyle, J. Orenstein, and J. G. Analytis, Electrical switching in a magnetically intercalated transition metal dichalcogenide, *Nat. Mater.* **19**, 153 (2020).
- [14] M. Iavarone, G. Karapetrov, J. Fedor, D. Rosenmann, T. Nishizaki, and N. Kobayashi, The local effect of magnetic impurities on superconductivity in Co_xNbSe₂ and Mn_xNbSe₂ single crystals, *J. Phys.: Condens. Matter* **22**, 015501 (2010).
- [15] M. Iavarone, G. Karapetrov, J. Fedor, and D. Rosenmann, The spectroscopic signature of the Co magnetic state in Co_xNbSe₂ superconducting single crystals, *Supercond. Sci. Technol.* **24**, 024010 (2011).
- [16] R. Pervin, A. Ghosh, H. Ghosh, and P. M. Shirage, Study of transport properties in Se-deficient and Fe-intercalated NbSe₂ single crystals: Experiment and theory, *J. Mater. Sci.* **55**, 250 (2020).
- [17] E. Berger, P. Valášek, and W. von der Linden, Two-dimensional Hubbard-Holstein model, *Phys. Rev. B* **52**, 4806 (1995).
- [18] R. T. Scalettar, N. E. Bickers, and D. J. Scalapino, Competition of pairing and Peierls-charge-density-wave correlations in a two-dimensional electron-phonon model, *Phys. Rev. B* **40**, 197 (1989).
- [19] M. Vekić, R. M. Noack, and S. R. White, Charge-density waves versus superconductivity in the Holstein model with next-nearest-neighbor hopping, *Phys. Rev. B* **46**, 271 (1992).
- [20] M. Vekić and S. R. White, Gap formation in the density of states for the Holstein model, *Phys. Rev. B* **48**, 7643 (1993).
- [21] M. Hohenadler, H. G. Evertz, and W. von der Linden, Quantum Monte Carlo and variational approaches to the Holstein model, *Phys. Rev. B* **69**, 024301 (2004).
- [22] M. Weber and M. Hohenadler, Two-dimensional Holstein-Hubbard model: Critical temperature, Ising universality, and bipolaron liquid, *Phys. Rev. B* **98**, 085405 (2018).
- [23] N. C. Costa, K. Seki, S. Yunoki, and S. Sorella, Phase diagram of the two-dimensional Hubbard-Holstein model, *Commun. Phys.* **3**, 80 (2020).
- [24] P. M. Dee, K. Nakatsukasa, Y. Wang, and S. Johnston, Temperature-filling phase diagram of the two-dimensional Holstein model in the thermodynamic limit by self-consistent Migdal approximation, *Phys. Rev. B* **99**, 024514 (2019).
- [25] O. Bradley, G. G. Batrouni, and R. T. Scalettar, Superconductivity and charge density wave order in the two-dimensional Holstein model, *Phys. Rev. B* **103**, 235104 (2021).
- [26] B. Cohen-Stead, N. C. Costa, E. Khatami, and R. T. Scalettar, Effect of strain on charge density wave order in the Holstein model, *Phys. Rev. B* **100**, 045125 (2019).
- [27] M. V. Araújo, J. P. de Lima, S. Sorella, and N. C. Costa, Two-dimensional $t - t'$ Holstein model, *Phys. Rev. B* **105**, 165103 (2022).
- [28] S. Li, E. A. Nowadnick, and S. Johnston, Quasiparticle properties of the nonlinear Holstein model at finite doping and temperature, *Phys. Rev. B* **92**, 064301 (2015).
- [29] P. M. Dee, J. Coulter, K. G. Kleiner, and S. Johnston, Relative importance of nonlinear electron-phonon coupling and vertex corrections in the Holstein model, *Commun. Phys.* **3**, 145 (2020).
- [30] G. Paleari, F. Hébert, B. Cohen-Stead, K. Barros, R. T. Scalettar, and G. G. Batrouni, Quantum Monte Carlo study of an anharmonic Holstein model, *Phys. Rev. B* **103**, 195117 (2021).
- [31] B. Xiao, N. C. Costa, E. Khatami, G. G. Batrouni, and R. T. Scalettar, Charge density wave and superconductivity in the disordered Holstein model, *Phys. Rev. B* **103**, L060501 (2021).
- [32] N. C. Costa, T. Blommel, W.-T. Chiu, G. Batrouni, and R. T. Scalettar, Phonon Dispersion and the Competition between Pairing and Charge Order, *Phys. Rev. Lett.* **120**, 187003 (2018).
- [33] Y. Wang, I. Esterlis, T. Shi, J. I. Cirac, and E. Demler, Zero-temperature phases of the two-dimensional Hubbard-Holstein model: A non-Gaussian exact diagonalization study, *Phys. Rev. Res.* **2**, 043258 (2020).
- [34] Z.-X. Li, M. L. Cohen, and D.-H. Lee, Enhancement of superconductivity by frustrating the charge order, *Phys. Rev. B* **100**, 245105 (2019).
- [35] R. Blankenbecler, D. J. Scalapino, and R. L. Sugar, Monte Carlo calculations of coupled boson-fermion systems. I, *Phys. Rev. D* **24**, 2278 (1981).
- [36] J. E. Hirsch, Discrete Hubbard-Stratonovich transformation for fermion lattice models, *Phys. Rev. B* **28**, 4059 (1983).
- [37] J. E. Hirsch, Two-dimensional Hubbard model: Numerical simulation study, *Phys. Rev. B* **31**, 4403 (1985).
- [38] N. Kawashima, Quantum Monte Carlo methods, *Prog. Theor. Phys. Suppl.* **145**, 138 (2002).
- [39] R. R. dos Santos, Introduction to quantum Monte Carlo simulations for fermionic systems, *Braz. J. Phys.* **33**, 36 (2003).
- [40] F. Becca and S. Sorella, *Quantum Monte Carlo Approaches for Correlated Systems* (Cambridge University Press, Cambridge, 2017).
- [41] R. K. Kaul, Spin Nematics, Valence-Bond Solids, and Spin Liquids in SO(N) Quantum Spin Models on the Triangular Lattice, *Phys. Rev. Lett.* **115**, 157202 (2015).
- [42] S. Gazit, F. F. Assaad, S. Sachdev, A. Vishwanath, and C. Wang, Confinement transition of \mathbb{Z}_2 gauge theories coupled to massless fermions: Emergent quantum chromodynamics and SO(5) symmetry, *Proc. Natl. Acad. Sci. USA* **115**, E6987 (2018).
- [43] T. Sato, F. F. Assaad, and T. Grover, Quantum Monte Carlo Simulation of Frustrated Kondo Lattice Models, *Phys. Rev. Lett.* **120**, 107201 (2018).
- [44] Z. H. Liu, X. Y. Xu, Y. Qi, K. Sun, and Z. Y. Meng, Itinerant quantum critical point with frustration and a non-Fermi liquid, *Phys. Rev. B* **98**, 045116 (2018).
- [45] A. S. Darmawan, Y. Nomura, Y. Yamaji, and M. Imada, Stripe and superconducting order competing in the Hubbard model on a square lattice studied by a combined variational Monte Carlo and tensor network method, *Phys. Rev. B* **98**, 205132 (2018).

- [46] S. R. White, D. J. Scalapino, R. L. Sugar, N. E. Bickers, and R. T. Scalettar, Attractive and repulsive pairing interaction vertices for the two-dimensional Hubbard model, *Phys. Rev. B* **39**, 839 (1989).
- [47] M. Ulmke, P. J. H. Denteneer, R. T. Scalettar, and G. T. Zimanyi, Enhancement of long-range antiferromagnetic order by nonmagnetic impurities in the Hubbard model, *Europhys. Lett.* **42**, 655 (1998).
- [48] L. Oliveira-Lima, N. C. Costa, J. P. de Lima, R. T. Scalettar, and R. R. dos Santos, Dynamical resilience to disorder: The dilute Hubbard model on the Lieb lattice, *Phys. Rev. B* **101**, 165109 (2020).
- [49] This weakening of the nearest-neighbor spin correlation functions is due to thermal effects.
- [50] D. Stauffer and A. Aharony, *Introduction To Percolation Theory*, 2nd ed. (Taylor & Francis, London, 1992).
- [51] R. Kubo, The fluctuation-dissipation theorem, *Rep. Prog. Phys.* **29**, 255 (1966).
- [52] R. Kubo, M. Toda, and N. Hashitsume, Statistical mechanics of linear response, in *Statistical Physics II: Nonequilibrium Statistical Mechanics* (Springer, Berlin, Heidelberg, 1991), pp. 146–202.
- [53] A. J. Kim, F. Simkovic, and E. Kozik, Spin and Charge Correlations across the Metal-to-Insulator Crossover in the Half-Filled 2D Hubbard Model, *Phys. Rev. Lett.* **124**, 117602 (2020).
- [54] M. Jarrell and J. E. Gubernatis, Bayesian inference and the analytic continuation of imaginary-time quantum Monte Carlo data, *Phys. Rep.* **269**, 133 (1996).